Rapid Gas-assisted Exfoliation Promises V_2O_5 Nanosheets for High Performance Lithium-sulfur Batteries

Chao Wang,[a, b, 1] Yikun Yi,[c, 1] Hongping Li,[b] Peiwen Wu,[b] Mingtao Li,[c,*] Wei Jiang,[b,d] Zhigang Chen,[a] Huaming Li,[b] Wenshuai Zhu,[b,*] Sheng Dai[e,*]

[a.] Institute of Environmental Health and Ecological Security, School of the Environment and Safety Engineering, Jiangsu University, 301 Xuefu Road, Zhenjiang 212013, P. R. China.

[b.] Institute for Energy Research, School of Chemistry and Chemical Engineering, Jiangsu University, 301 Xuefu Road, Zhenjiang 212013, P. R. China. E-mail: zhuws@ujs.edu.cn.

[c.] School of Chemical Engineering and Technology, Xi'an Jiaotong University, 28 West Xianning Road, Xi'an 710049, P. R. China. E-mail: lmt01558@mail.xjtu.edu.cn.

[d.] Department of Chemistry, University of Tennessee, Knoxville 37996, USA.

[e.] Chemical Sciences Division, Oak Ridge National Laboratory, Oak Ridge 37831, USA. E-mail: dais@ornl.gov.

[1] These authors contributed equally.

Key Words: gas-assisted exfoliation, vanadium pentoxide, nanosheets, lithium-sulfur batteries

Abstract: Scalable synthesis of ultra-thin two-dimensional (2D) nanomaterials by exfoliation has emerged as an intriguing approach in the energy field. Herein, a rapid thermal expansion-triggered gas-assisted exfoliation method is applied to synthesize ultra-thin 2D V_2O_5 nanosheets. Unlike other methods, no impurities can be introduced during exfoliation, leading extremely clean 2D nanosheets that are crucial in the investigation of 2D materials in charge-storage fields. The obtained V_2O_5 nanosheets were used as effective host materials for polysulfides in lithium-sulfur batteries, as they can help to confine and alleviate the shuttle of polysulfides efficiently. The as-prepared V_2O_5-S composite electrode delivered an initial discharge capacity of 1638.5 mAh g^{-1} with a high Coulombic efficiency of 96.7% and maintained a specific capacity of 838.8 mAh g^{-1} after 200 cycles at 0.1 C current rate. This work supplies a facile approach to obtain transition metal oxide nanosheets, which have potential applications in energy storage and conversion fields.

1. Introduction

Rechargeable lithium-sulfur (Li-S) batteries with outstanding theoretical specific capacity (1675.0 mAh g^{-1}) and energy density (2600.0 Wh kg^{-1}) are attracting considerable attentions because they are promising candidates for mobile devices and electric vehicles.[1-5] Unfortunately, their implementation has been hindered by several issues: (1) the insulating properties of S and lithium sulfide, (2) the notorious shuttling of the polysulfides, and (3) huge volume fluctuations (≈ 80%). These issues can result in low S utilization, poor Coulombic efficiency and rapid capacity decline, respectively.[6-11] However, these problems arise mainly from the dissolution of reaction intermediates (Li_2S_n, $4 \leq n \leq 8$) in the electrolyte. A series of commonly used methods have been developed to deal with the issues mentioned, for instance, (1) incorporating S into host materials with high specific surface areas and abundant polar sites and (2) applying functional interlayers and binders. Among numerous candidates, carbon materials are the ones most often selected to construct S cathodes because of their excellent conductivity and adjustable porosity.[12-15] However, owing to the weak interactions between the polysulfides species and non-polar carbon, the confinement of polysulfides is unsatisfied here.

As reviewed by Nazar and Zhang,[16-17] transition metal oxides (TMOs, such as V_2O_5, MnO_2, Co_3O_4 and CuO) have redox potentials above a certain range (i.e., ≥ 2.4 V) could chemically bond polysulfides on the surfaces of reduced metal oxides, which are favorable candidates for S cathodes. Moreover, the abundant polar sites on the surfaces of TMOs could help to adsorb polysulfides in organic electrolytes effectively.[18-19] Among the TMOs mentioned, V_2O_5 might be one of the most suitable candidates owing to its higher redox potentials (>3.0 V) and stronger surface polarity. Based on Cui's theoretical calculation,[20] V_2O_5 with a layered structure exhibits strong chemical interaction with Li_2S_n clusters, indicating that V_2O_5 nanosheets might be a promising candidate for Li-S batteries. Additionally, two-dimensional (2D) ultra-thin layered structure materials are promising hosts for S cathodes, as their abundant active binding sites and high specific surface areas are beneficial for the constraint of generated polysulfides.[21-25] Traditional solvothermal methods are reliable for preparing

2D V_2O_5 nanosheets with the addition of various organic solvents in the reaction kettle.[26-27] However, this process requires long time, high temperature and high pressure conditions, making it hard to obtain scalable V_2O_5 nanosheets. In addition, volatile toxic organic solvents are used in this process, necessitating subsequent complicated separation and purification steps. Thus, rapid synthesis of V_2O_5 nanosheets under mild conditions without the use of volatile toxic solvents merits investigation.[28-31]

Herein, an efficient, nontoxic thermal expansion-triggered gas-assisted exfoliation method for rapid preparation of 2D ultra-thin V_2O_5 nanosheets is introduced with using commercially available bulk V_2O_5 as precursor (Scheme 1). It is worth noting that the volume of the V_2O_5 powder after exfoliation increased sharply based on the same mass. The whole procedure did not use any traditional volatile toxic organic solvents. With this facile exfoliation method, extremely clean V_2O_5 nanosheets (< 3 nm) could be obtained, as no impurities would be introduced during exfoliation process. Besides, it achieved ~50% yield in a short time under relatively ambient conditions, which is superior to previous works.[26-27, 32] Specifically, the introduction of the exfoliated V_2O_5 nanosheets can help to constrain polysulfides in the electrolyte effectively, and Li-S batteries based on V_2O_5-S composite electrode can deliver a high initial discharge specific capacity (1638.5 mAh g^{-1}) and a long cycle life (838.8 mAh g^{-1} after 200 cycles).

Scheme 1. Rapid gas-assisted exfoliation of bulk V_2O_5 into ultra-thin V_2O_5 nanosheets.

2. Experimental Section

2.1 Materials synthesis

2.1.1 Preparation of V_2O_5 nanosheets

All the starting materials were of analytical grade and used as received. First of all, 2 g commercially available bulk V_2O_5 (Alfa Aesar) was placed in a ceramic crucible. Then, they were heated in a 600 °C muffle furnace for at least 5 min. After this, the heated V_2O_5 was immediately dropped into a Dewar bottle, which containing liquid nitrogen (L-N_2). The remained V_2O_5 was collected after the L-N_2 evaporated totally. Then, the above steps were repeated 15 cycles. When the former steps were finished, the obtained powder was dispersed in ethanol. After this, the mixture was sonicated for 30 min. Any possible remaining bulk precursors were separated out by centrifugation. The centrifugal rate and centrifugal time were 4000 rpm and 1 minute, respectively. Finally, V_2O_5 nanosheets were obtained after evaporating ethanol in the collected supernatant fluid. The yield of V_2O_5 nanosheets is finally determined by the weight ratio between the obtained V_2O_5 nanosheets and original bulk V_2O_5, and its value is around 50%. Safety issues for the preparation of V_2O_5 nanosheets are listed in Supporting Information.

2.1.2 Synthesis of V_2O_5-S composites

Sulfur encapsulation was performed *via* a melt-diffusion method. The as-prepared V_2O_5 nanosheets (0.1g) and sulfur (0.15g) were mixed together and hand-milled for about 30 min. Then, the mixture was transferred to an electric oven at 155 °C for 16 h. Upon cooling, the powder was collected. And the theoretical sulfur content was 50%, according to the TGA result.

2.1.3 Preparation of Li_2S_6 solution

The Li_2S_4 solution was prepared *via* a hydrothermal method. Briefly, 160 mg sulfur and 46 mg Li_2S were mixed in 10 mL mixture electrolyte of DOL and DME (1:1 volume ratio) and magnetic stirred for 1 h. Then, the solution was heated at 60 ˚C for 12 h under the argon atmosphere.

2.2 Electrochemical measurements

The electrochemical measurements were carried out by galvanostatic cycling in a CR2016-type coin cell. The cathode was prepared by mixing 80 wt% of the active material (V_2O_5-S), 10 wt% acetylene black and 10 wt% of polyvinylidene fluoride (PVDF) in N-methyl pyrrolidinone (NMP) to form a homogeneous slurry. Then, the slurry was uniformly spread onto an aluminum foil with the active material loading of about 1.2 mg cm^{-2}. The interlayer slurry for V_2O_5-S cathode was prepared by mixing 80 wt% of C_3N_4, 10 wt% of graphene, and 10 wt% PVDF in NMP solution. The slurry was coated onto the surface of V_2O_5-S cathode electrode, with a thickness of 13 μm (according to the SEM image in Figure S1) and an average mass of 0.7 mg on each cathode. Finally, the electrode film was dried at 60 °C in a vacuum oven overnight and then cut into round disks with a diameter of 12 mm for coin cell assembling. The 2016-type coin cells were assembled in an argon-filled glove box (Mikrouna Co.) with low levels of H_2O and O_2 (H_2O < 0.01 ppm, O_2 < 0.01 ppm). Li metal (a thickness of 1.4 mm and a diameter of 16 mm) and Celgard 2400 membrane were used as anode and separator, respectively. The electrolyte solution was 1 M bis (trifluoromethane) sulfonimide lithium salt (LiTFSI) in 1,3-dioxolane (DOL) and 1,2-dimethoxyethane (DME) (volume ratio 1:1) with 1 wt% $LiNO_3$, with 50 μL used in one cell. The cells were galvanostatically discharged and charged using a CT2001A cell test instrument (LAND Electronic Co.) at room temperature between 1.7 and 2.6 V at different current densities, and the specific capacities were calculated based on the sulfur as the cathode-active material. Then, cyclic voltammetry (CV) was carried out on a CHI 760D electrochemistry workstation with a scan rate of 0.1 mV s^{-1} from 1.7 to 2.6 V (*vs* Li^+/Li).

2.3 Assemble of S-free batteries and Li_2S_6 symmetric batteries

Briefly, the V_2O_5 electrodes were prepared by mixing V_2O_5 samples (bulk or nano), acetylene carbon (AB) and PVDF in NMP with a weight ratio of 8:1:1. The uniform slurry was coated on an aluminum foil and dried at 60 °C for 12 h, and then cut into disks with a diameter of 12 mm. The S-free batteries were assembled as the same procedure with V_2O_5-S batteries, just using V_2O_5 electrodes instead of V_2O_5-S cathodes. As for Li_2S_6 symmetric batteries, two identical V_2O_5 disks (bulk V_2O_5 or V_2O_5

nanosheets) were used as both working and counter electrodes. 50 μL of Li_2S_6 solution (0.1 M) was added as electrolyte and Celgard 2400 membrane was used as separator, respectively. Another cell without Li_2S_6 in electrolyte was also assembled as a control. Then, CV curves of symmetric cells were carried on an electrochemical workstation with a scan rate of 10 mV s^{-1} between -1 and 1 V.

3. Results and discussion

To prove the successful generation of ultra-thin V_2O_5 nanosheets with this gas-assisted exfoliation strategy, electron microscopy analyses were conducted initially. In Figure S2, the transmission electron microscopy (TEM) images of bulk V_2O_5 show irregular rod-shaped particles with a length of ~5 μm. While, in Figure 1a, the high-resolution TEM (HRTEM) image of V_2O_5 nanosheets exhibit a terraced structure, indicating effective delamination in the gas-assisted exfoliation process.[28] In Figure 1b, the six parallel fringes or stripes observed at the edge of V_2O_5 nanosheets correspond to the six stacked layers in the samples.[33-36] As can be seen in the HRTEM and selected area electron diffraction (SAED) images in Figure 1c, the structure of V_2O_5 nanosheets remains ordered after gas-assisted exfoliation.[33] Moreover, a clear Tyndall light scattering effect can still be observed in V_2O_5 nanosheets colloidal suspension over a week, indicating the formation of stable ultra-thin V_2O_5 nanosheets (Figure 1d).[37-39] The thickness of the V_2O_5 nanosheets was subsequently measured by atomic force microscopy (AFM, Figure 1e-1g). Both the corresponding three-dimensional (3D) demonstration (Figure 1f) and the thickness profiles along lines I, II, III, and IV (Figure 1g) indicate that the thickness of the as-prepared nanosheets is mainly less than 3 nm. Given that the thickness of a single-layer V_2O_5 is about 0.44 nm,[40] it was concluded that the number of V_2O_5 layers was not more than seven.

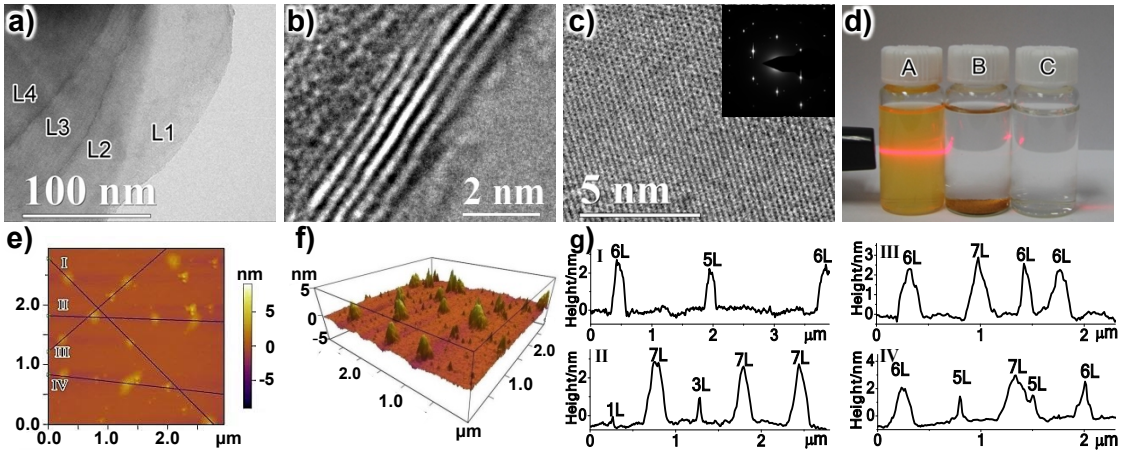

Figure 1. Characterizations of exfoliated V_2O_5 nanosheets. (a) HRTEM image of V_2O_5 nanosheets. (b) HRTEM image of the edge folding of V_2O_5 nanosheets with six layers. (c) HRTEM and SAED images of V_2O_5 nanosheets. (d) Tyndall effect of the as-prepared V_2O_5 nanosheets (A: V_2O_5 nanosheets, B: bulk V_2O_5, C: ethanol). (e) AFM image of V_2O_5 nanosheets. (f) 3D demonstration of V_2O_5 nanosheets. (g) The corresponding height profiles of V_2O_5 nanosheets (I, II, III and IV), "L" denotes layer.

The structure of the V_2O_5 nanosheets was further analyzed by X-ray powder diffraction (XRD) measurement. Figure 2a illustrates a typical structure of bulk V_2O_5 with lattice parameters of a = 11.52 Å, b = 3.57 Å, c = 4.37 Å (JCPDS card 41-1426). However, only one obvious diffraction peak ((001) facets) was observed with exfoliated ultra-thin V_2O_5 nanosheets. The decreased intensity of other peaks (like the (200), (110), and (301) facets) illustrates the reduced stacking in the c-direction.[28, 41] In addition, the corresponding two-theta (2θ) degree shifts from 20.26° to 20.13° (Figure 2b), indicating an increased interplanar distance (d-spacing) from 4.37 to 4.41 Å. Both the disappeared diffraction peaks and increased d-spacing helped to confirm the formation of ultra-thin V_2O_5 nanosheets. Then, the specific surface area of exfoliated V_2O_5 nanosheets was estimated by the Brunauer-Emmett-Teller (BET) method (Figure S3). Compared with bulk precursor, the specific surface area of exfoliated V_2O_5 nanosheets is 8.6 times larger than that of bulk V_2O_5 (19.8 m^2/g *vs.* 2.3 m^2/g). The increased specific surface area of V_2O_5 nanosheets would expose more polar sites, which could help to suppress the migration of polysulfides efficiently. Besides, high-resolution X-ray photoelectron spectroscopy (XPS) analysis of the V_2O_5 nanosheets (Figure S4) shows agreement with the spectra of bulk V_2O_5,[42] indicating that the structure of V_2O_5 is stable during the gas-

assisted exfoliation process.

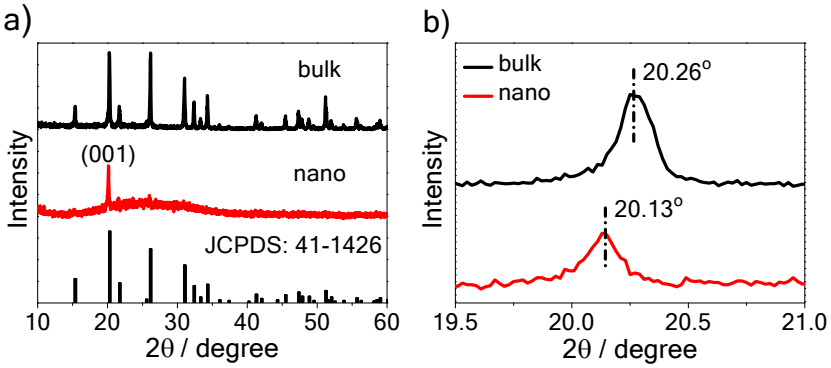

Figure 2. XRD patterns of bulk V_2O_5(bulk) and V_2O_5 nanosheets (nano).

Additionally, to demonstrate the changing features of bulk V_2O_5 and its ultra-thin structure, the as-prepared nanosheets were characterized by Fourier transform infrared spectroscopy (FT-IR) and Raman spectroscopy. The point symmetry group of V_2O_5 (*Pmmn* (59)) belongs to D_{2h}, and the model structures of the V-O layers are displayed in Figure S5. In the D_{2h} group, the FT-IR active mode and Raman active mode are represented as B_{1u}, B_{2u}, B_{3u} and A_g, B_{1g}, B_{2g}, B_{3g} by Bouckaert-Smoluchowski-Wigner (BSW) notation according to the irreducible representations, respectively.[43] Then, all peaks observed were assigned by the above irreducible representations (Figure 3, Figure S6).[44-45] In a classical harmonic oscillator model, effective restoring forces acting on the atoms would be decreased from bulk materials to ultra-thin nanosheets, leading the phonons to be soften. This phenomenon can be explained by the decrease of the interlayer van der Waals interactions from bulk materials to ultra-thin nanosheets. Hence, these seven groups of peaks in the nanosheets should exhibit some red shifts. Moreover, density functional theory (DFT) calculation results also indicate that red shifts of the peaks would occur in a thinner material (Figure S7, detailed discussions are provided in the Supporting Information). Upon analysis of the obtained spectral data (Figure 3, Table S1), red shifts were indeed observed in the V_2O_5 nanosheets, further indicating that ultra-thin nanosheets can be prepared successfully with the foregoing gas-assisted exfoliation method.[46-47]

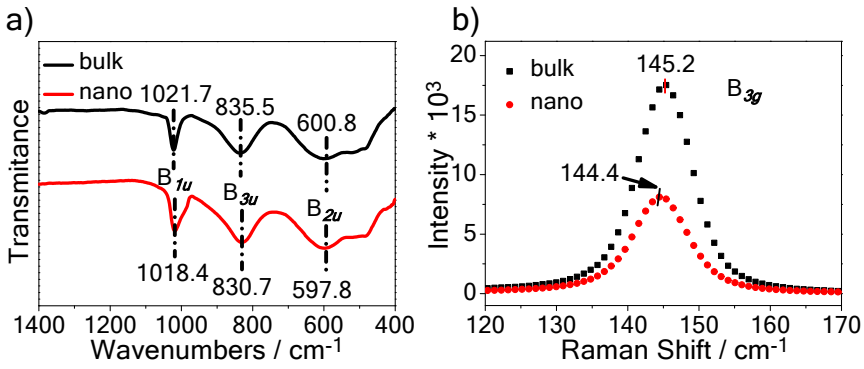

Figure 3. Structure characterization of bulk V_2O_5 (bulk) and V_2O_5 nanosheets (nano): (a) FT-IR, (b) Raman.

The electrochemical performances of the V_2O_5 nanosheets-S (**abbreviated as "V_2O_5-S"**) cathode were evaluated in CR2016 coin cells. The as-prepared ultra-thin V_2O_5 nanosheets exhibited favorable properties in Li-S batteries. Typical cyclic voltammetry (CV) curves of the V_2O_5-S cathode (*vs.* Li^+/Li) are presented in Figure 4a for the first five cycles with a scanning rate of 0.1 mV s^{-1}. The two reduction peaks at 2.29 and 2.01 V are closely related to the conversion of Li_2S_n ($4 \leq n \leq 8$) and the final formation of insoluble Li_2S_2/Li_2S, respectively. In addition, two prominent oxidation peaks located at 2.33 and 2.40 V are observed, corresponding to the reverse reactions of polysulfides. Moreover, the position shift of those peaks in the five CV curves is negligible, illustrating the favorable cycling stability of Li-S batteries.

Galvanostatic charge and discharge tests were also carried at different current densities. Figure 4b shows cycling performance of V_2O_5-S cathode at 0.1 C, with an initial discharge capacity of 1437.1 mAh g^{-1}. To eliminate the extra capacity contribution of V_2O_5 nanosheets, a pure V_2O_5 cell without sulfur species was fabricated under the same condition. The discharge profiles and cycling capacities are displayed in Figure S8, which exhibits an initial discharge capacity of 292.3 mAh g^{-1} between 1.7 and 2.6 V and subsequent stable capacity of 40.6 mAh g^{-1}, indicating that the contribution of V_2O_5 nanosheets to the capacity of Li-S batteries could be rationally ignored except during the initial cycle. Then, charge and discharge profiles of batteries at 0.1 C are shown in Figure 4c. The two plateaus in the discharge profiles are consistent with the two respective reduction peaks in the CV curves. In comparison to V_2O_5-S

cathode, the V_2O_5(bulk)-S electrode delivers an initial capacity of only 705.2 mAh g^{-1} and even sharply drops to 275.7 mAh g^{-1} at the 5th cycle, owing to the disappearance of the second discharge plateau during cycling. The capacity contribution of bulk V_2O_5 could also be ignored according to Figure S8. This result distinctly demonstrates a better application of V_2O_5 nanosheets than bulk V_2O_5 in Li-S batteries, which is mainly attributed to the increased specific surface area and more exposed polar sites, as they can chemically bond polysulfides effectively. Besides, a CV test of [bulk V_2O_5/bulk V_2O_5] and [V_2O_5 nanosheets/V_2O_5 nanosheets] symmetric cells was also carried to further investigate the role of V_2O_5 nanosheets, using two identical S-free disks (bulk V_2O_5 or V_2O_5 nanosheets) as working and counter electrodes. As shown in Figure S9, the cell without Li_2S_6 exhibits a horizontal line, eliminating the influence of capacitive contribution. V_2O_5 nanosheets@Li_2S_6 cell delivers distinctly larger redox current response and peaks than bulk V_2O_5@Li_2S_6 cell, verifying a favorable catalytic effect for accelerating kinetics of polysulfide conversion, which could also be related to the increased polar sites on the surface of V_2O_5 nanosheets.

Then, to further improve the batteries performances of V_2O_5-S, a carbon nitride and graphite (CNG) interlayer was applied on the cathode. It has been proposed to effectively enhance cycling performance based on our previous work,[48] as it could effectively suppress diffusion of polysulfides. Notably, coated with CNG interlayer, the V_2O_5-S electrode (V_2O_5-S-CNG) delivers an ultra-high initial capacity of 1638.5 mAh g^{-1} at 0.1 C with a high Coulombic efficiency of 96.7% (Figure 4d). Furtherly, when the current density increased to 0.2, 0.5, and 1 C, this cathode exhibits capacities of 925.3, 836.8 and 751.4 mAh g^{-1}, respectively, and it still maintains a reversible capacity of 891.8 mAh g^{-1} when the rate is directly switched to 0.1 C (Figure 4d). Moreover, the V_2O_5-S-CNG electrode displays remarkable cycling performance. As shown in Figure 4e, it exhibits a specific capacity of 838.8 mAh g^{-1} after 200 cycles at 0.1 C, in contrast to 495.2 mAh g^{-1} for the cathode without a C_3N_4/G coating interlayer (Figure 4b). At a current density of 0.5 C (Figure 4f, Figure S10), the V_2O_5-S-CNG cell shows a first cycle discharge specific capacity of 932.8 mAh g^{-1} and a charge capacity of 961.3 mAh g^{-1} with a high Coulombic efficiency of 97.0%. Moreover, it maintained an invertible

specific capacity of 713.3 mAh g^{-1} even after 150 cycles with 76.5% capacity maintenance, delivering remarkable cycling stability.

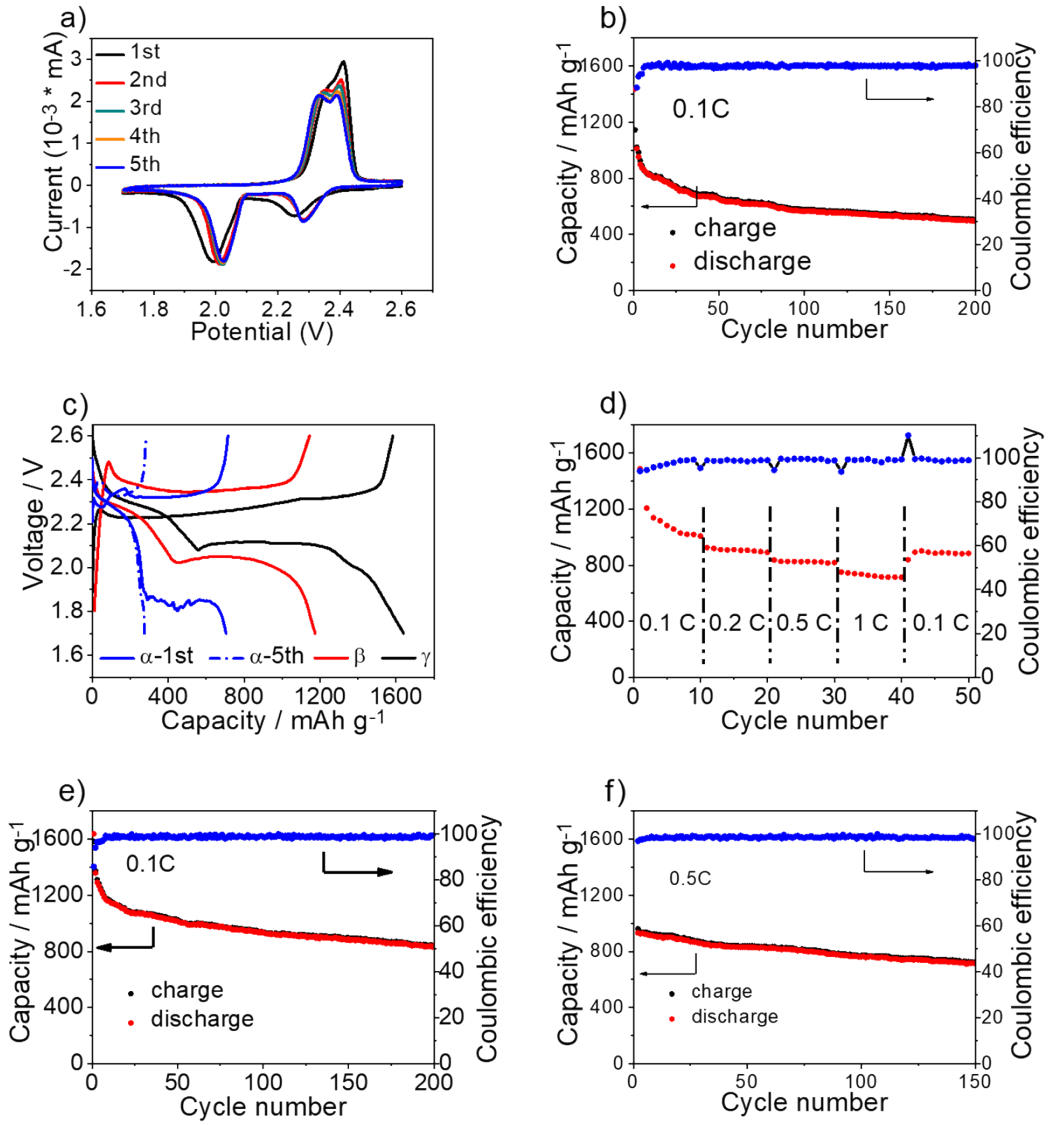

Figure 4. Electrochemical characterization of V_2O_5-S as a cathode for Li-S batteries. (a) CV measured between 1.7 and 2.6 V (*vs*. Li^+/Li) for V_2O_5-S at a scanning rate of 0.1 mV s^{-1}. (b) Cycling performances and Coulombic efficiencies of V_2O_5-S cathodes at 0.1 C. (c) Galvanostatic discharge-charge profiles for different electrodes at 0.1 C (α: V_2O_5 (bulk)-S electrode, β: V_2O_5-S electrode, γ: V_2O_5-S-CNG electrode). Capacity was calculated by the mass of sulfur. (d) Rate performance of discharge-charge capacity at various rates. (e) Cycling performances and Coulombic efficiencies of V_2O_5-S-CNG cathodes at 0.1 C. (f) Cycling performances and Coulombic efficiencies of V_2O_5-S-CNG cathodes at 0.5 C.

4. Conclusions

Ultra-thin V_2O_5 nanosheets were obtained *via* a rapid thermal expansion-triggered

gas-assisted exfoliation method. The obtained nanosheets were not more than seven atomic layers thick. Owing to the distinctly increased polar sites from the surface of nanosheets, polysulfides in the electrolyte could be confined efficiently. The V_2O_5-S composite electrode delivered a high initial discharge specific capacity of 1638.5 mAh g^{-1} at 0.1 C current rate, and it retained a specific capacity of 838.8 mAh g^{-1} after 200 cycles at 0.1 C current rate. This work not only provides a novel electrode material as a host for S cathodes in high-energy-density and long-cycle-life Li-S batteries, but also shares new insight for the production of few-layer TMOs (like MnO_2, MoO_3, WO_3 or TiO_x), which can be used in the fields of Li-S batteries, selective catalytic reduction reactions, water splitting, CO_2 activation and many other areas.

Acknowledgments

The authors appreciate the financial support from the National Natural Science Foundation of China (Nos. 21722604, 21808092 and 21978231), the Natural Science Foundation of Shaanxi Province in China (No. 2017ZDJC-30), Fundamental Research Funds for the Central Universities in China. S. D. was supported by U.S. Department of Energy, Office of Science, Office of Basic Energy Sciences, Materials Sciences and Engineering Division.

Appendix A. Supplementary data

Supplementary data to this article can be found online.

References

1. B.Y. Hao, H. Li, W. Lv, Y.B. Zhang, S.Z. Niu, Q. Qi, S.J. Xiao, J. Li, F.Y. Kang, Q.H. Yang, Nano Energy 60 (2019) 305-311.
2. X.L. Ji, S. Evers, R. Black, L.F. Nazar, Nat. Commun. 2 (2011) 325.
3. X.J. Liu, N. Xu, T. Qian, J. Liu, X.W. Shen, C.L. Yan, Nano Energy 41 (2017) 758-764.
4. A. Manthiram, Y.Z. Fu, S.H. Chung, C.X. Zu, Y.S. Su, Chem. Rev. 114 (2014) 11751-11787.

5. C. Ye, Y. Jiao, H.Y. Jin, A.D. Slattery, K. Davey, H.H. Wang, S.Z. Qiao, Angew. Chem. Int. Ed. 57 (2018) 16703-16707.
6. S.F. Wang, Y. Ding, G.M. Zhou, G.H. Yu, A. Manthiram, ACS Energy Lett. 1 (2016) 1080-1085.
7. G.G. Eshetu, X. Judez, C.M. Li, M. Martinez-Ibañez, I. Gracia, O. Bondarchuk, J. Carrasco, L.M. Rodriguez-Martinez, H. Zhang, M. Armand, J. Am. Chem. Soc. 140 (2018) 9921-9933.
8. L.Y. Du, Q. Wu, L.J. Yang, X. Wang, R.C. Che, Z.Y. Lyu, W. Chen, X.Z. Wang, Z. Hu, Nano Energy 57 (2019) 34-40.
9. Z.L. Ma, S. Dou, A.L. Shen, L. Tao, L.M. Dai, S.Y. Wang, Angew. Chem. Int. Ed. 54 (2015) 1888-1892.
10. C. Ye, L. Zhang, C.X. Guo, D.D. Li, A. Vasileff, H.H. Wang, S.Z. Qiao, Adv. Funct. Mater. 27 (2017) 1702524.
11. X.J. Fan, W.W. Sun, F.C. Meng, A.M. Xing, J.H. Liu, Green Energy Environ. 3 (2018) 2-19.
12. G.Q. Tan, R. Xu, Z.Y. Xing, Y.F. Yuan, J. Lu, J.G. Wen, C. Liu, L. Ma, C. Zhan, Q. Liu, Nat. Energy 2 (2017) 17090.
13. Z.L. Ma, L. Tao, D.D. Liu, Z. Li, Y.Q. Zhang, Z.J. Liu, H.W. Liu, R. Chen, J. Huo, S.Y. Wang, J. Mater. Chem. A 5 (2017) 9412-9417.
14. J.C. Ye, J.J. Chen, R.M. Yuan, D.R. Deng, M.S. Zheng, L. Cronin, Q.F. Dong, J. Am. Chem. Soc. 140 (2018) 3134-3138.
15. X. Song, S.Q. Wang, Y. Bao, G.X. Liu, W.P. Sun, L.X. Ding, H.K. Liu, H.H. Wang, J. Mater. Chem. A 5 (2017) 6832-6839.
16. X. Liang, C.Y. Kwok, F. Lodi-Marzano, Q. Pang, M. Cuisinier, H. Huang, C.J. Hart, D. Houtarde, K. Kaup, H. Sommer, T. Brezesinski, J. Janek, L. F. Nazar, Adv. Energy Mater. 6 (2016) 1501636.
17. X. Liu, J.Q. Huang, Q. Zhang, L.Q. Mai, Adv. Mater. 29 (2017) 1601759.
18. X. Song, G.P. Chen, S.Q. Wang, Y.P. Huang, Z.Y. Jiang, L.X. Ding, H.H. Wang, ACS Appl. Mater. Interfaces 10 (2018) 26274-26282.
19. J. Zhang, Y. Shi, Y. Ding, W.K. Zhang, G.H. Yu, Nano Lett. 16 (2016) 7276-7281.

20. Q.F. Zhang, Y.P. Wang, Z.W. Seh, Z.H. Fu, R.F. Zhang, Y. Cui, Nano Lett. 15 (2015) 3780-3786.
21. Z. Li, J.T. Zhang, X.W. Lou, Angew. Chem. Int. Ed. 54 (2015) 12886-12890.
22. H.Q. Wang, T.F. Zhou, D. Li, H. Gao, G.P. Gao, A.J. Du, H.K. Liu, Z.P. Guo, ACS Appl. Mater. Interfaces 9 (2016) 4320-4325.
23. H. Hu, B.T. Zhao, H.Y. Cheng, S.G. Dai, N. Kane, Y. Yu, M.L. Liu, Nano Energy 57 (2019) 635-643.
24. W. Yang, W. Yang, A.L. Song, G. Sun, G.J. Shao, Nanoscale 10 (2018) 816-824.
25. G.P. Chen, X. Song, S.Q. Wang, X.Z. Chen, H.H. Wang, J. Power Sources 408 (2018) 58-64.
26. S.Q. Liang, Y. Hu, Z.W. Nie, H. Huang, T. Chen, A.Q. Pan, G.Z. Cao, Nano Energy 13 (2015) 58-66.
27. A.Q. Pan, H.B. Wu, L. Zhang, X.W. Lou, Energy Environ. Sci. 6 (2013) 1476-1479.
28. W.S. Zhu, X. Gao, Q. Li, H.P. Li, Y.H. Chao, M.J. Li, S.M. Mahurin, H.M. Li, H.Y. Zhu, S. Dai, Angew. Chem. Int. Ed. 55 (2016) 10766-10770.
29. W.S. Zhu, Z.L. Wu, G.S. Foo, X. Gao, M.X. Zhou, B. Liu, G.M. Veith, P.W. Wu, K.L. Browning, H.N. Lee, H.M. Li, S. Dai, H.Y. Zhu, Nat. Commun. 8 (2017) 15291.
30. P.W. Wu, J. He, L.L. Chen, Y.C. Wu, H.P. Li, H.Y. Zhu, H.M. Li, W.S. Zhu, J. Energy Chem. 27 (2018) 1509-1515.
31. Y.C. Wu, P.W. Wu, Y.H. Chao, J. He, H.P. Li, L.J. Lu, W. Jiang, B.B. Zhang, H.M. Li, W.S. Zhu, Nanotechnology 29 (2018) 025604.
32. X.H. Rui, Z.Y. Lu, H. Yu, D. Yang, H.H. Hng, T.M. Lim, Q.Y. Yan, Nanoscale 5 (2013) 556-560.
33. W.W. Lei, V.N. Mochalin, D. Liu, S. Qin, Y. Gogotsi, Y. Chen, Nat. Commun. 6 (2015) 8849.
34. X.B. Fan, P.T. Xu, Y.C. Li, D.K. Zhou, Y.F. Sun, M.A.T. Nguyen, M. Terrones, T.E. Mallouk, J. Am. Chem. Soc. 138 (2016) 5143-5149.
35. M.T. Li, W.S. Zhu, P.F. Zhang, Y.H. Chao, Q. He, B.L. Yang, H.M. Li, A.

Borisevich, S. Dai, Small 12 (2016) 3535-3542.

36. H.H. Ou, L.H. Lin, Y. Zheng, P.J. Yang, Y.X. Fang, X.C. Wang, Adv. Mater. 29 (2017) 1700008.
37. C.L. Tan, P. Yu, Y.L. Hu, J.Z. Chen, Y. Huang, Y.Q. Cai, Z.M. Luo, B. Li, Q.P. Lu, L.H. Wang, Z. Liu, H. Zhang, J. Am. Chem. Soc. 137 (2015) 10430-10436.
38. Y. Xu, W.W. Zhao, R. Xu, Y.M. Shi, B. Zhang, Chem. Commun. 49 (2013) 9803-9805.
39. J.Q. Tian, Q. Liu, C.J. Ge, Z.C. Xing, A.M. Asiri, A.O. Al-Youbi, X.P. Sun, Nanoscale 5 (2013) 8921-8924.
40. X.F. Zhang, K.X. Wang, X. Wei, J.S. Chen, Chem. Mater. 23 (2011) 5290-5292.
41. X.B. Fan, P.T. Xu, D.K. Zhou, Y.F. Sun, Y.C. Li, M.A.T. Nguyen, M. Terrones, T.E. Mallouk, Nano Lett. 15 (2015) 5956-5960.
42. H.M. Zeng, D.Y. Liu, Y.C. Zhang, K.A. See, Y.S. Jun, G. Wu, J.A. Gerbec, X.L. Ji, G.D. Stucky, Chem. Mater. 27 (2015) 7331-7336.
43. L.P. Bouckaert, R. Smoluchowski, E. Wigner, Phys. Rev. 50 (1936) 58-67.
44. R. Baddour-Hadjean, V. Golabkan, J.P. Pereira-Ramos, A. Mantoux, D. Lincot, J. Raman Spectrosc. 33 (2002) 631-638.
45. P. Clauws, J. Broeckx, J. Vennik, Phys. Status Solidi B 131 (1985) 459-473.
46. C. Lee, H. Yan, L.E. Brus, T.F. Heinz, J. Hone, S. Ryu, ACS Nano 4 (2010) 2695-2700.
47. X.H. Ren, J. Zhou, X. Qi, Y.D. Liu, Z.Y. Huang, Z.J. Li, Y.Q. Ge, S.C. Dhanabalan, J.S. Ponraj, S.Y. Wang, J.X. Zhong, H. Zhang, Adv. Energy Mater. 7 (2017) 1700396.
48. L. Qu, P. Liu, Y.K. Yi, T. Wang, P. Yang, X.L. Tian, M.T. Li, B.L. Yang, S. Dai, ChemSusChem 12 (2019) 213-223.

Chao Wang received his Ph.D. degree in environmental science and engineering from Jiangsu University (P.R. China) in 2018. He is currently an assistant researcher at Jiangsu University. His current research focuses on design and synthesis of 2D materials for energy conversion.

Yikun Yi received his B.S. degree in chemical engineering and technology from Xi'an Jiaotong University (P.R. China) in 2017. He is currently an M.S. candidate under the supervision of Prof. Mingtao Li at Xi'an Jiaotong University. His current research focuses on design and synthesis of cathode substrates for lithium-sulfur batteries.

Hongping Li received his Ph.D. degree in physical chemistry from Xiamen University (P.R. China) in 2012. He is currently an associate professor at Jiangsu University. His current research focuses on computational chemistry, ionic liquids and 2D materials.

Peiwen Wu received his Ph.D. degree in power engineering and engineering thermophysics from Jiangsu University in 2018. He has joined Prof. Dr. Sheng Dai's group as a visiting scholar from Nov. 2016 to Apr. 2018 at Oak Ridge National Laboratory (ORNL, USA). He is currently a lecturer at Jiangsu University. His current research focuses on design and synthesis of 2D materials for clean utilization of fossil energies.

Mingtao Li received his Ph.D. degree in chemical engineering from Shanghai Jiao Tong University (P.R. China) in 2011. He has joined Prof. Dr. Sheng Dai's group as a visiting scholar from Aug. 2014 to Aug. 2015 at ORNL. He is currently an associate professor at Xi'an Jiaotong University. His current research interests in the synthesis of cathodes and solid electrolytes for lithium-ion batteries and lithium-sulfur batteries.

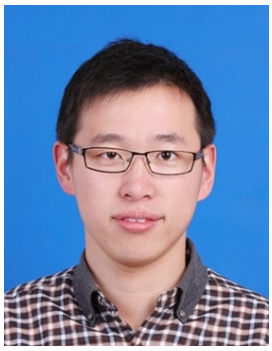

Wei Jiang received his Ph.D. degree in clean energy and environmental protection from Jiangsu University in 2014. He is currently an associate researcher at Jiangsu University and also a visiting scholar at the University of Tennessee (USA). His current research focuses on the synthesis of 2D materials for application in clean energy.

Zhigang Chen received his Ph.D. degree in environmental engineering from Jiangsu University in 2008. He is currently a full professor at Jiangsu University. His current research activities encompass nanocomposites for clean energy and energy storage devices.

Huaming Li received his M.S. degree in physical chemistry from Chinese Academy of Sciences (P.R. China) in 1992. He is currently a full professor at Jiangsu University. His current research focuses on nanomaterials and ionic liquids for energy and environmental applications. He has published over 500 peer-reviewed journal papers with more than 16,000 total citations and an h-index of 71.

Wenshuai Zhu received his Ph.D. degree in environmental engineering from Jiangsu University in 2009. He has joined Prof. Dr. Sheng Dai's group as a visiting scholar from Jan. 2015 to Jun. 2016 at ORNL. He is currently a full professor at Jiangsu University. His current research focuses on nanomaterials (especially 2D nanosheets) and ionic liquids for energy and environmental applications. He has published over 160 peer-reviewed journal papers with more than 5,000 total citations and an h-index of 40.

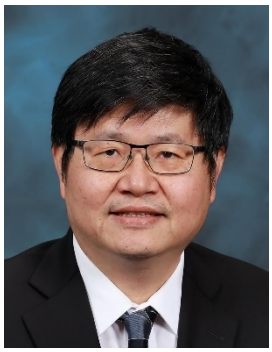

Sheng Dai received his Ph.D. degree in chemistry from the University of Tennessee in 1990. He is currently a corporate fellow (the highest designation a researcher can receive at ORNL) and a group leader at the ORNL and a professor of Chemistry at the University of Tennessee, Knoxville. His current research interests include ionic liquids, porous carbon and oxide materials, advanced materials and their applications for separation sciences and energy storage as well as catalysis by nanomaterials. He has published over 800 peer-reviewed journal papers with more than 35,000 total citations and an h-index of 96.